Separation and Purification Technology 237 (2020) 116386

Contents lists available at ScienceDirect

Separation and Purification Technology

journal homepage: www.elsevier.com/locate/seppur

High viscosity preparative chromatography for food applications

A. Schultze-Jena[a,b], M.A. Boon[a,*], R.C. Vroon[a], P.J.Th. Bussmann[a], A.E.M. Janssen[b], A. van der Padt[b,c]

[a] Food and Biobased Research, Wageningen University and Research, Wageningen, The Netherlands
[b] Food Process Engineering, Wageningen University and Research, Wageningen, The Netherlands
[c] FrieslandCampina, Amersfoort, The Netherlands

ARTICLE INFO

Keywords:
Preparative chromatography
Productivity
Viscosity
System size
Food fractionation

ABSTRACT

The strength of chromatography lies in the ability of fine-tuning recovery for specific target components or fractions of interest. A downside of industrial chromatography is the need to dilute streams, as it is often applied today. This article challenges the conventional low concentration of input streams and investigates size exclusion chromatography at concentrated streams of high viscosity. Chromatographic operation with concentrated streams leads to an increased pressure drop over the column and decreased mass transfer kinetics, but also lower volumes compared to diluted streams. The objective of this research was to investigate separation performance and system dimensions as a function of viscosity for food type streams, in scenarios where viscosity is not caused by target components. Disadvantages due to increased stream volume with decreasing concentration and benefits due to decreased viscosity were evaluated, aiming to find minimal column volume.

Separation performance was evaluated for a range of target components in a preparative lab-scale system using a size exclusion resin and mobile phase viscosities in the range of 1.2–8.7 mPa·s. Mobile phases were viscosified through addition of sucrose, glycerol, or dextran. Change in mass transfer resistance, measured via *van Deemter* curves, was related to the change in diffusivity through viscosity.

The analysis of different viscosifying agents emphasized the influence of viscosity inside the pores, rather than viscosity of the bulk phase. The viscosity inside the pores was calculated via the partition coefficient of each viscosifying agent. Based on the slopes of *van Deemter* curves, column dimensions were calculated for different scenarios, assuming a non-compressible stationary phase. Column volume remained constant with stream dilution from 8.7 mPa·s down to about 2.5 mPa·s. However, at the same time column geometry changed to thinner and longer columns with decreasing viscosity, in order to accommodate throughput and pressure drop. When diluting to even lower viscosities, column volume increased, since stream viscosity is less sensitive to stream concentration at the low viscosity range. These results are relevant to a wide range of industries utilizing weak interaction chromatography, especially those where the main driver of process development is cost reduction and where a trade-off between purity, yield, and costs has to be made.

1. Introduction

Preparative chromatographic separations distinguish themselves from most other separation techniques through the ability to fine-tune separation mechanisms for specific molecular properties of target components. This ability allows access to fractions of interest with low loss of product, high purity, and high productivity. In order to economize chromatography in industrial processes, process productivity is optimized in regard to product loss, processing time, and unit costs. Productivity, generally defined as ratio of product mass to column volume and processing time, is commonly improved by optimizing product yield and/or processing time. Additional potential for productivity optimization lies within reduction of column volume. Column volume is directly linked to chromatographic resin and eluent quantities required, which in many separation processes are the main contributors to overall chromatographic footprint and processing costs and can be reduced if column volume is reduced [1]. One possibility to reduce column volume is reduction of feed stream volume by operation at higher concentrations. But, with increase in concentration, most streams will also show an increase in viscosity, which in turn will have a negative impact on both mass transfer and pressure drop. Commonly, processes are designed to keep stream viscosity as low as possible in

* Corresponding author.
E-mail address: floor.boon@wur.nl (M.A. Boon).

https://doi.org/10.1016/j.seppur.2019.116386
Received 9 July 2019; Received in revised form 29 November 2019; Accepted 1 December 2019
Available online 03 December 2019

order to maximize diffusion and chromatographic efficiency and minimize retention times [2].

Literature on the effect of mobile phase viscosity in liquid column chromatography is primarily concerned with *viscous fingering*, a phenomenon which reduces column efficiency through instable interfaces between liquid phases of different viscosities [3,4]; if all liquid phases have the same viscosity, as in this work, viscous fingering does not occur. The effects of viscosity on mass transfer inside chromatographic columns have been discussed to a limited extent. Colin et al. looked at the change in mobile phase viscosity through temperature [5]. They found the main effect of increased temperature on column efficiency and pressure drop is due to the reduced viscosity, which leads to increased diffusivities of the target components. Nakanishi et al. described the dispersion of NaCl and glucose in size exclusion chromatography, focusing on diffusion inside a range of *Sephadex* stationary phases [6]. In one part of their work the mobile phase was viscosified with added glycerol to a viscosity of 2.5 mPa·s and elution curves of NaCl were measured. The increase in viscosity resulted in an increase in mass transfer resistance. This study builds on the work done by Nakanishi et al. [6]. The mobile phase viscosity was increased even further, up to 8.7 mPa·s.

In general, there are three scenarios where operating at higher stream viscosity may theoretically lead to direct benefits in separation processes. First, inherently viscous streams are diluted before chromatographic processing, only to remove water content of product fractions in subsequent steps. If costly and energy intensive removal of water was minimized by reducing dilution prior to chromatographic separation, process cost savings would be imminent. Second, streams with large volumes and low concentration of target components are often discarded entirely and their product content is not utilized. If the stream volume was reduced, less volume with a higher product concentration could make the purification of target components economically feasible, despite water removal costs. For both scenarios, a chromatographic step under increased viscosity could lead to smaller column volumes and thus processing cost reduction. In a third scenario, chromatography at elevated viscosity may be a viable alternative to chromatography at high temperatures. Many components of complex products are sensitive to temperature and require mild treatment throughout the process. In all three scenarios column length and column diameter will change with input stream viscosity and volume. Relating column volume to bulk viscosity leads to optimized process conditions and minimized water use.

Evaluation of column volume with changing mobile phase viscosity requires knowledge on column efficiency, stream viscosity, and pressure drop over the column bed, when input stream concentration is changed. Column efficiency is evaluated based on the number of plates N, which can be determined as a requirement for a given separation process [5]. The number of plates in a chromatographic column is defined by the ratio of column length L over the height equivalent to a theoretical plate *HETP*. With the term *HETP*, fluid dynamic non-idealities, mass transfer resistances, and ad- and desorption rates in a chromatographic column are summed up [5]. One of the most prominent factors on *HETP* is the diffusion of molecules in mobile and stationary phases, in the latter especially at preparative scale. Molecular diffusivity is directly related to mobile phase properties such as viscosity, temperature, and concentration of its constituents, as well as molecular size or volume of the diffusing molecule itself. Diffusivity in a stationary phase is a more complex matter, but generally speaking it is related to diffusivity in the mobile phase and reduced through (steric) hindrances induced by the porous stationary phase [6]. The influence of concentration on stream viscosity is known for most simple solutions and can be measured in more complex cases. The pressure drop in packed chromatographic beds as a function of viscosity is known. The main unknown is the influence of viscosity on *HETP*, described by the *van Deemter* curve.

This study builds on the work done by Colin et al. and Nakanishi et al. [5,6]. The temperature was kept constant and the mobile phase viscosity was increased through addition of viscosifying agents. The effect of viscosity on *HETP* and system volume was analyzed under the condition that not the target component but the viscosifying agent caused the bulk viscosity. The focus was laid on plate height and the change in number of plates, however the authors are aware that the required number of plates for a separation depends on peak shapes as well. *Van Deemter* curves, which relate *HETP* to velocity, were measured at various viscosities. Mobile phase viscosity was increased with three different viscosity agents: sucrose, a common constitute of many food streams such as ketchup, juices, and extracts, was compared to glycerol and dextran to analyze influence of molecular characteristics of the viscosifying agent. A new method is demonstrated that enables the comparison of column designs for different stream concentrations based on a constant number of plates and pressure drop. With this method, the influence of viscosity and viscosifier concentration was related to the number of plates N and changes in column dimensions. This research aims at a variety of industries such as food processing or polymer production as well as other processes, where processing costs are limiting factors and, unlike for pharmaceutical requirements, the optimal combination of purity, yield, and costs is a trade-off.

2. Theory

2.1. Height equivalent to a theoretical plate as a function of viscosity

Preparative chromatography at large scale generally utilizes high velocities to treat large stream volumes and rather large particle diameters to maintain a low pressure drop over the column bed. In such conditions, linear interstitial velocity u_L and particle diameter d_p are easily a hundred times larger, compared to typical analytical chromatography. When velocity and particle diameter are so large, overall *HETP* in weak interaction chromatography processes is typically dominated by transparticle mass transfer resistance H_{Stat} [7], which in turn is proportional to the quotient of interstitial linear velocity u_L and intraparticle diffusivity D_p (Eq. (1)).

$$HETP\ H_{Stat} \propto \frac{u_L}{D_p} \tag{1}$$

Intraparticle diffusivity D_p is a function of solute interaction with stationary phase properties, here summed up as Ω, and solute diffusivity in the liquid phase inside the pore volume $D_{m.pore}$ (Eq. (2)) [8].

$$D_p = \Omega \cdot D_{m \cdot pore} \tag{2}$$

When mobile phase viscosity is influenced by viscosifying agents, solute diffusivity inside pore volume $D_{m.pore}$ may not be identical to solute diffusivity in the bulk phase $D_{m.bulk}$. Within the pore volume, molecules are confined by the ratio of their size to pore diameter. This confinement influences the concentration of all molecules in pore volumes and may cause mobile phase viscosity to be different in pore volumes than in the bulk phase. The concentration inside the pores as function of mobile phase concentration can be determined via isotherm measurements. For linear relationships of concentration in bulk and pore, the concentration ratio of each molecule between pore and bulk can be expressed via the partition coefficient K_D (Eq. (3)) [9].

$$K_D = \frac{c_{pore}}{c_{bulk}} \tag{3}$$

The partition coefficient K_D of the viscosity agent can be determined from pulse injection measurements of retention volume of the viscosifying agent V_R, the interparticle void volume V_0 and the total mobile phase volume V_T (Eq. (4)) in phosphate buffer without elevated viscosity [10].

$$K_D = \frac{V_R - V_0}{V_T - V_0} \tag{4}$$

From the concentration of the viscosifying agent in the mobile phase, concentration inside pore volumes is determined and used to calculate an average viscosity μ_{pore} in the pore volume. Solute diffusivity $D_{m.i}$ (cm^2/s) in turn is inversely proportional to viscosity μ_i (either in the bulk or inside the pore), as given by the Wilke-Chang equation (Eq. (5)) [2,11].

$$D_{m\cdot i} = \frac{7.4\cdot 10^{-8}(\varphi M_{B\cdot i})^{1/2} T}{\mu_i V_A^{0.6}} \tag{5}$$

With φ, the dimensionless association factor of 2.6 for water, $M_{B.i}$ molecular weight of the bulk phase (mixture of phosphate buffer and viscosifier; g/mol), T temperature (K), μ_i viscosity in the bulk or inside the pore volume (mPa·s) and V_A molecular volume of solute at boiling point (mL/mol), calculated after *Le Bas* [11].

Combining Eqs. (1), (2), and (5), shows that a change of *HETP* as function of velocity under preparative conditions is proportional to inverse $D_{m.pore}$, which in turn is inversely proportional to the viscosity inside the pores μ_{pore}, leading to the relationship of Eq. (6):

$$\frac{HETP}{u_L} \propto \frac{1}{D_{m.pore}} \Rightarrow \frac{HETP}{u_L} \propto \mu_{pore} \tag{6}$$

Change in *HETP* as function of u_L is plotted as *van Deemter* curve and its determination standard chromatographic procedure. Generally *van Deemter* plots are normalized by dividing *HETP* by the resin particle diameter d_p, which yields the reduced HETP h and the linear interstitial velocity u_L is multiplied by d_p and divided by $D_{m.bulk}$, which yields the reduced velocity ν.

2.2. Column dimensions as a function of mobile phase viscosity

This method enables calculation of column dimensions for different bulk viscosities on the basis of fixed parameters such as a constant pressure drop, required number of plates, and initial stream volume.

Column length L and operating velocity u_S are calculated for a constant pressure drop Δp and a specific viscosity (solid green line in Fig. 1). The same parameters L and u_S are calculated for a constant number of plates N at that same viscosity (dashed blue line in Fig. 1). The intersection of the two lines, marks the operating parameters at which all requirements are met, when utilizing a specific stream viscosity (red circle in Fig. 1).

Column length for a constant pressure drop over the column bed as function of velocity is calculated with the *Ergun* equation (Eq. (7)), with column length L (m), pressure drop Δp (Pa), mobile phase viscosity μ_{bulk} (Pa·s), particle diameter d_p (m), bed porosity ε_b (−), mobile phase density ρ (kg/m^3), and superficial linear velocity u_S (m/s) [12].

$$\frac{1}{L} = \frac{150\mu_{bulk}}{d_p^2 \Delta p}\frac{(1-\varepsilon_b)^2}{{\varepsilon_b}^3}u_S + \frac{1.75\rho}{d_p \Delta p}\frac{(1-\varepsilon_b)}{{\varepsilon_b}^3}u_S^2 \tag{7}$$

Eq. (7) is valid only in case of a non-compressible stationary phase. Many industrially relevant stationary phases do exhibit compression to a certain degree, dependent on operating conditions and column aspect ratios, which must be considered when scaling designs. For such a case Stickel and Fotopoulos derived adjustments to empirical models to correlate pressure drop to aspect ratio of packed beds and velocity and further predict bed porosity [13]. As a first approximation for scale-up, we assumed the stationary phase was non-compressible.

Column length for a constant number of plates as function of linear superficial velocity u_S is calculated based on slopes of *van Deemter* curves and Eq. (8) with $u_L = u_S/\varepsilon_b$.

$$L = HETP(u_L)\cdot N \tag{8}$$

Column volume CV is calculated from L and column area A, which in turn was calculated by dividing volumetric stream Q_V with linear superficial velocity u_S. The stream volume Q_V is reduced with stream concentration.

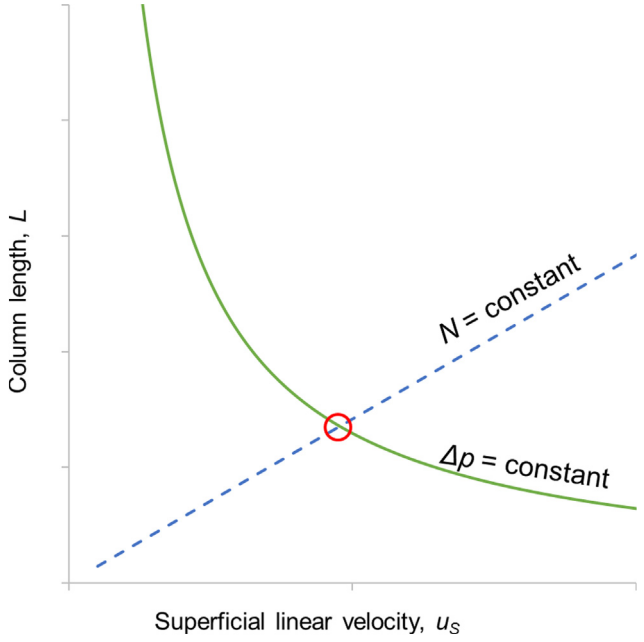

Fig. 1. Column length L and superficial linear velocity u_S for set parameters and a specific viscosity. Solid green line shows operation at constant pressure drop over the column Δp, dashed blue line shows operation at constant number of plates N. Intersection of both lines, marked with red circle, gives L and u_S at set pressure drop and plate number for a specific viscosity. (For interpretation of the references to colour in this figure legend, the reader is referred to the web version of this article.)

With this method the column volume for operation at any given viscosity can be calculated, as long as the *van Deemter* curve, the pressure drop over the column bed, and the viscosifier concentration are known.

3. Materials and methods

3.1. Materials

3.1.1. Mobile phase

All experiments were conducted with a phosphate buffered mobile phase (25 mM Na_2HPO_4, 25 mM NaH_2PO_4, and 50 mM NaCl; all from Merck, Germany) in Milli-Q water. Viscosity was increased by use of sucrose, a small dextran of 9–11 kDa (both from Sigma Aldrich, St. Louis, MO, USA) or glycerol (Boom, the Netherlands). For the viscous mobile phases, the viscosifier was dissolved first and the salts were added according to the volume of the solution. For each mobile phase the viscosity was measured with a Physica MCR 301 rheometer (Anton Paar, Austria) at 22 °C. Viscosities and concentration of viscosifier added are detailed in Table 3.1.

Before use mobile phases were filtered through a 0.45 µm Durapore® membrane filter (Merck, Germany). Between experiments mobile phases were stored at 4 °C, but no longer than 48 h before use.

Table 3.1
Concentration of sucrose and glycerol (% m/m) to reach target viscosities in each mobile phase.

Viscosifier\Viscosity	1.2 mPa·s	2.3 mPa·s	4.5 mPa·s	8.7 mPa·s
Sucrose	0%	22%	–	44%
Glycerol	0%	–	46%	58%
Dextran	0%	–	19%	27.5% (8.0 mPa·s)

Table 3.2
Target components, concentration in sample volume and *UV* detection wavelength (*RI* for refractive index).

Target	c (g/L)	Detection
γ-aminobutyric acid	3	210 nm
Triglycerin	1	218 nm
Glycyl-L-tyrosine	1	276 nm
Dextran	10	RI
NaCl	58	200 nm
Acetone	2% v/v	260 nm

3.1.2. Stationary phase

All experiments were conducted using Sephadex G-15 size exclusion resin (GE Healthcare, Uppsala, Sweden) with a cut off of about 1.5 kDa, according to the manufacturers website. The mean particle diameter (80 μm) was measured with a Mastersizer 2000 (Malvern, UK).

3.1.3. Target component preparation

All solid target components were dissolved in the mobile phase at each viscosity, to avoid any changes in viscosity along the column and associated phenomena like viscous fingering. All target components were from Sigma Aldrich, St. Louis, MO, USA. Respective target concentrations and detection wavelengths (refractive index in case of dextran) are given in Table 3.2. Acetone was the only liquid target component and added per volume.

3.1.4. Chromatographic equipment

For liquid chromatography a Wellchrom set-up with a K–1001 pump and a K-2401 RI–detector was used, all from Knauer, Germany. Furthermore a Julabo F25 MP controlled the temperature in the column jacket and a mini Cori-Flow flowmeter (Bronkhorst, The Netherlands) measured the flow rate after the detector. Pressure drop over the column bed was continuously measured using EZG10 pressure sensors (Knauer, Germany), all components were connected with 0.02″ PEEK tubing (Grace, Deerfield, IL, USA).

Column measurements were made on a slurry packed *Götec* Superformance 300–10 column (300 × 10 mm) with *tefzel* capillaries of 35 cm lengths and ID 0.5 mm, including flow adapter with frits and filter (all Götec, Germany). During all experiments bed height and pressure drop were recorded and, if required, flow adapters adjusted to minimize headspace upon bed compression or the bed repacked. The zero length column was a *Götec* Superformance 10–10 column (10 × 10 mm) with no resin and the flow adapters in direct contact as described in [14].

3.2. Methods

3.2.1. Column preparation and characterization

For experiments at low viscosity, the column was slurry packed in two steps. The first began with phosphate buffer to settle the slurry in a ramped up profile of up to 10 mL/min for 20 min. In the second step the funnel for the slurry packing was removed, the flow adapter and a filter placed above the resin bed and the resin bed further compressed at 10 mL/min for 30 min. For measurements at high viscosity, the column was slurry packed in three steps. First, resin slurry was settled in a ramped up flow profile of up to 10 mL/min for 20 min in phosphate buffer. Second, mobile phase was exchanged to 8.7 mPa·s sucrose phosphate buffer and flow reduced to 3 mL/min for 25 min. Third, the funnel for the slurry packing was removed, the flow adapter and a filter placed above the resin bed and the resin bed compressed at 3 mL/min in 8.7 mPa·s sucrose phosphate buffer for 30 min. External porosity was measured via retention volume of 10 g/L dextran (average molecular weight of approximately $2 \cdot 10^6$ Da) pulse injections in phosphate buffer and with blue-dextran (both Sigma Aldrich, St. Louis, MO, USA) at higher viscosities (*UV* detection at 621 nm).

3.2.2. Chromatographic analysis

All chromatographic measurements were conducted as pulse injections of 80 μL at varying velocity. The column was kept at 22 °C through a water jacket. All peaks were analyzed with the method of moments in Microsoft Excel as described in [14]. Integration limits were set automatically at 1% of total peak height and baseline drift was corrected for automatically when necessary to mitigate common concerns of inaccuracy when using the method of moments [15–17]. A detailed example of the correction of drifting baselines and the setting of peak start and end points is given in the supplementary material for *γ-aminobutyric acid* in different mobile phases (Fig. 12a through 12e). With high viscosifier concentration some target components showed a low signal intensity in their chromatogram, resulting in detection instabilities, noisy baselines, and sometimes minima before or after the peak. Among the elution peaks in the supplementary material (Fig. 13), *γ-aminobutyric acid* eluted in sucrose and glycerol gives a good example of aforementioned detection challenges (Fig. 13b). In these cases the integration limits were set manually. Linear superficial velocities u_S were 0.5, 1, 2, and 3 m/h (0.5, 1, 1.5, and 2 m/h with dextran as viscosifier at 4.5 mPa·s and 8 mPa·s). With each new mobile phase the column was equilibrated with a minimum of five column volumes. All measurements were corrected for extra-column contribution for each mobile phase viscosifier, viscosity, velocity, and target component, as described in [14].

3.2.3. Measurement of partition coefficient – K_D

The partition coefficient K_D for sucrose and glycerol was calculated from the slopes of linear isotherms. Isotherms were measured via frontal analysis of breakthrough times with the staircase method via the refractive index (RI) as described by [18]. To the unviscosified phosphate buffer the viscous mobile phase was added in steps of 5% (v/v), while the viscous mobile phase was at the same viscosifier concentration as the maximum used in the pulse injection measurements.

K_D of all three mobile phase viscosifiers was additionally calculated with Eq. (4) from mean retention times measured from pulse injections of 80 μL at 1 m/h in unviscosified phosphate buffer as mobile phase. V_0 was measured with dextran ($2 \cdot 10^6$ Da) and V_T with 2% (v/v) acetone. K_D of dextran was measured from pulse injections and calculated with Eq. (4).

3.2.4. Mobile phase viscosity

Mobile phase viscosity was increased through addition of sucrose, glycerol, or dextran. Viscosity of different viscosifier concentrations in phosphate buffer were measured in a rheometer at 22 °C and functions fitted to the data. Viscosity of sucrose solutions was fitted to Eq. (9), a modification of an empirical model [19]. Viscosity of glycerol solutions was estimated using equations 10 through 15, as proposed by [20]. Viscosity of dextran solutions was fitted to Eq. (16), entirely based on measurements. Measurements, empirical models and fitted functions are shown in Fig. 11 which, along with Eqs. (9) through (16), can be found in the supplementary material.

3.2.5. Van Deemter curves and intraparticle diffusivity D_p

Van Deemter curves, *HETP* as function of linear interstitial velocity u_L, were recorded for each target component and mobile phase. From the slope in the linear region of each *van Deemter* curve the intraparticle diffusivity D_p was calculated as described in [7]. This method also takes the resistance to external mass transfer k_{film} into account, which was calculated using the Wilson and Geankoplis relation. Non-interacting conditions were assumed. The confidence interval of D_p was calculated from the propagated uncertainties of the slope of *van Deemter* curves and k_{film}. The uncertainty of the slope was calculated from the standard error of the slope with a 95% confidence interval, the uncertainty of k_{film} was estimated assuming an uncertainty of 20% for D_m.

Table 3.3
Case parameters for comparison of change in column dimensions with increased viscosity.

Name	Symbol	Quantity	Unit
Pressure drop	Δp	5	bar
Initial stream volume	Q_V	10	m^3/h
Number of plates	N	100	–
Particle size	d_p	80	µm
Temperature	T	22	°C
Bed porosity	ε_b	0.34	–

3.2.6. Parameters for system size calculations

The influence of the bulk viscosity on the system size is illustrated by separation of two minor components (target component and a component without affinity for the resin) in a viscous medium. For the calculation of column dimensions as function of viscosity, case parameters were set. All case parameters are given in Table 3.3. For the calculation of pressure drop, a bed porosity of 0.34 was assumed, even though *van Deemter* curves at higher viscosities were recorded with lower bed porosities.

An initial stream volume of 10 m^3/h and a viscosifier concentration of 1% (m/m) was assumed. Change in stream volume through water removal and subsequent increase in viscosity, was simulated by increasing concentration of viscosifying agent in the mobile phase while assuming a linear isotherm for all target components.

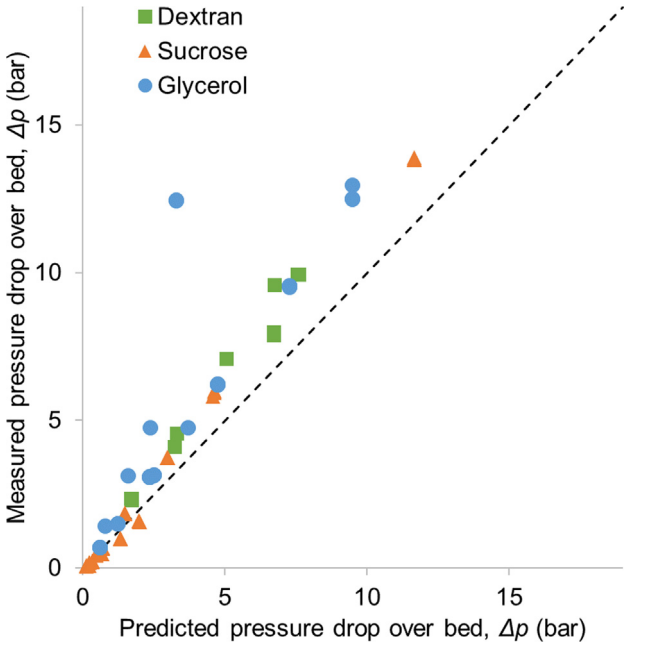

Fig. 3. Measured pressure drop over the column bed over the calculated pressure drop from Eq. (7). Pressure drop of mobile phase viscosified with dextran was constantly larger than expected due to higher apparent viscosity.

4. Results and discussion

4.1. Van Deemter curves at increased viscosities

Chromatography in viscous solutions leads to a decrease in overall mass transfer, resulting in increased slopes of *van Deemter* curves, as shown for *triglycine* in phosphate buffer viscosified to 2.3 and 8.7 mPa·s with sucrose in Fig. 2a and viscosified to 4.5 and 8.7 mPa·s with glycerol in Fig. 2b. Recording elution peaks in viscous mobile phases, two main effects and several side effects were observed. The first main effect was the expected increase in band broadening due to increased mass transfer resistance with viscosity. The second main effect was the degree of band broadening increase was correlated to the viscosity inside the pores, rather than the viscosity of the bulk phase; a topic further discussed in Section 4.2.

The observed side effects challenged experimental HETP determination and ultimately decreased accuracy with increasing viscosity. At lower viscosities, measured data points of the *van Deemter* curve formed a straight line with little or no deviation, visible from the small 95% confidence interval displayed by dotted lines in Fig. 2. At higher viscosities of the mobile phase recorded *van Deemter* curves showed a larger spread of data points for expected linear behavior, leading to larger uncertainty in determined slopes, which could be improved through additional measurements. As pressure drop increased, the resin bed compressed slightly, resulting in different bed heights, bed porosities, and retention volumes, which were corrected for in each case. Measured pressure drop was compared to the calculated pressure drop, which was calculated based on actual bed height and porosity with Eq.

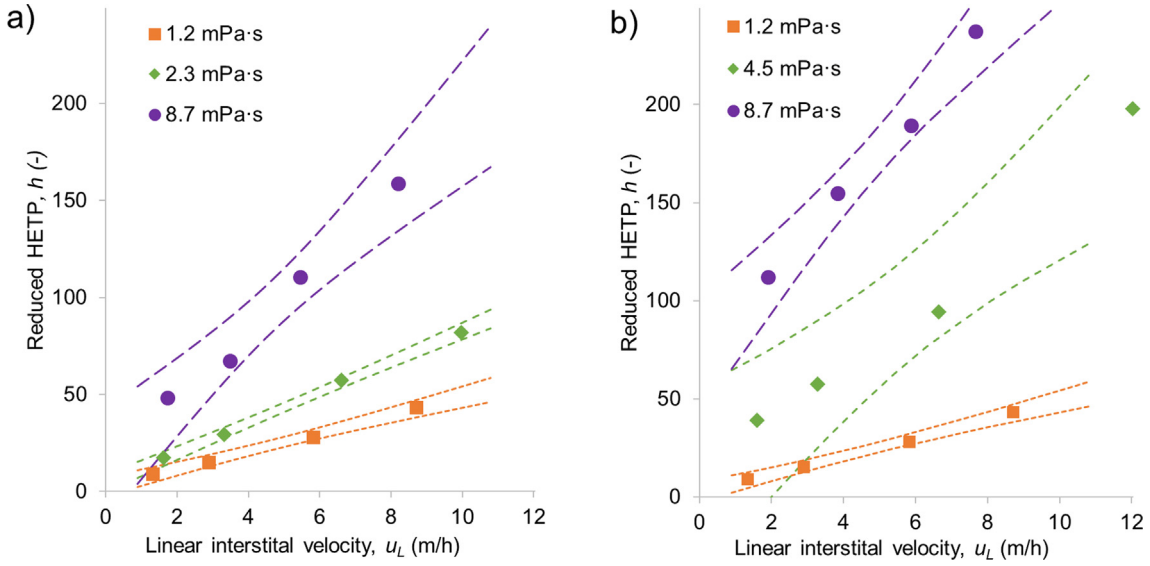

Fig. 2. *Van Deemter* curves of reduced HETP h over interstitial linear velocity u_L for *triglycine* in phosphate buffer at 1.2 mPa·s and (a) phosphate buffer containing sucrose at 2.3 and 8.7 mPa·s and (b) phosphate buffer containing glycerol at 4.5 and 8.7 mPa·s. Lines indicate 95% confidence interval for linear regression of the slope.

(7) (Fig. 3). In most cases measured pressure drop matched expected pressure drop fairly well. One measurement in glycerol, where measured pressure drop was far above expectation, led to a repacking of the column, as indicated in Fig. 3. Peak shapes changed from almost perfect symmetry to tailing and in some cases fronting peaks. Because of the focus of this work, the change in peak shape was not further analyzed, although it has an influence on *HETP* and an accurate description of the change in peak shape is important for application towards a practical separation. The elution peaks of acetone show an increase of retention volume with viscosity (average increase of retention volume by 5% with sucrose and 14% with glycerol in the mobile phase, both at 8.7 mPa·s, Fig. 13a), while all other retention volumes decrease (Fig. 13b–d). It is possible, that the high viscosifier concentrations lead to a reduced miscibility of the ternary systems (water, sucrose, acetone or water, glycerol, acetone) [21,22]. This change in solubility may have altered the adsorption equilibrium and subsequently acetone was retained longer in the stationary phase. Last but not least baseline stability decreased, resulting in necessity for baseline correction in some cases, especially for *γ–aminobutyric acid* measured at a wavelength of 210 nm (Fig. 13b). Elution peaks of *acetone*, *γ–aminobutyric acid*, *triglycine*, and *glycyl-L-tyrosine* at u_S = 1 m/h in phosphate buffer, and mobile phase viscosified with sucrose at 2.3 and 8.7 mPa·s and glycerol at 4.5 and 8.7 mPa·s are added to the supplementary material (Fig. 13).

For all investigated target components the following relationships were found: the larger the molecule, the steeper the slope of the *van Deemter* curve at low viscosity and greater the increase in slope with increased viscosity. *Van Deemter* curves of all target components showed similar behavior in terms of increasing confidence interval with viscosity (supplementary material, Figs. 14–16).

Comparison of peak broadening for different target components at different viscosities is best demonstrated by plotting reduced HETP h over reduced velocity ν which takes bulk diffusion coefficients into account (Fig. 4a for sucrose and Fig. 4b for glycerol in mobile phase). The slope of h over ν increased with molecular size, but due to the correction for the bulk diffusion coefficient $D_{M,bulk}$, displayed an almost linear behavior for each molecule with varying viscosities. But it is also evident from Fig. 4, that at high viscosity overall mass transfer resistance is not exactly proportional anymore to the diffusion coefficient in the bulk mobile phase, as slopes at 8.7 mPa·s differ from slopes at lower viscosities.

4.2. Influence of the partition coefficient of the viscosifying agent

A direct comparison of *van Deemter* curves for mobile phases viscosified with sucrose and glycerol revealed a difference in slope at the same mobile phase bulk viscosity (round symbols for 8.7 mPa·s in Fig. 4a and Fig. 4b). The same bulk viscosity resulted in a difference in slope and therefore a different resistance to overall mass transfer. From the slope of the *van Deemter* curve, the overall resistance to mass transfer was calculated, as described in [7], which takes into account both the mass transfer resistance inside the particle and outside the particle in the stationary film layer. The contribution of the film mass transfer resistance k_{film}, as calculated by the Wilson and Geankoplis relation, to the overall mass transfer resistance was negligible. Since bulk diffusivities in sucrose and glycerol were almost identical and overall mass transfer was dominated by the contribution of transparticle mass transfer, it stands to reason that the major difference between mass transfer in mobile phases viscosified with sucrose or glycerol affected diffusion inside the particle pores. Inside the pore volume, steric restriction imposed by the pore structure lead to a different distribution of viscosifier molecules between external and internal particle space, resulting in different viscosities, and thus diffusivities, in the pore volume. The difference in viscosity inside the pore and dependence of overall mass transfer not only on bulk viscosity, but also the viscosifiers ability to penetrate pore volume, was shown when dextran was introduced; a viscosifying agent too large to penetrate any pore volume.

The concentration of viscosifier molecules, and with that an averaged viscosity inside the pore volume, was calculated from the isotherms of sucrose and glycerol (Fig. 5). Since the isotherms are linear, the concentration can also be calculated via the partition coefficient K_D (Eq. (3)). The measured K_D values for sucrose and glycerol were 0.48 and 0.70 respectively. Measured K_D from pulse injections match the slope of isotherms for sucrose and glycerol. The isotherm of dextran showed an increase in stationary phase concentration at higher mobile phase concentration (Fig. 5), which cannot be explained through pore penetration, as the dextran used is about an order of magnitude larger than the cut off of the resin. A pore concentration of zero, as measured via the partition coefficient was assumed for the remainder of the experiments with dextran in the mobile phase. Viscosity inside the pore volume, calculated from the partition coefficient, is plotted as a function of bulk viscosity in Fig. 6. In addition to glycerol and sucrose, Fig. 6 also shows the pore viscosity for dextran with a K_D of 0 (no access to any pore volume) and the case for a K_D of 1 (complete access to pore

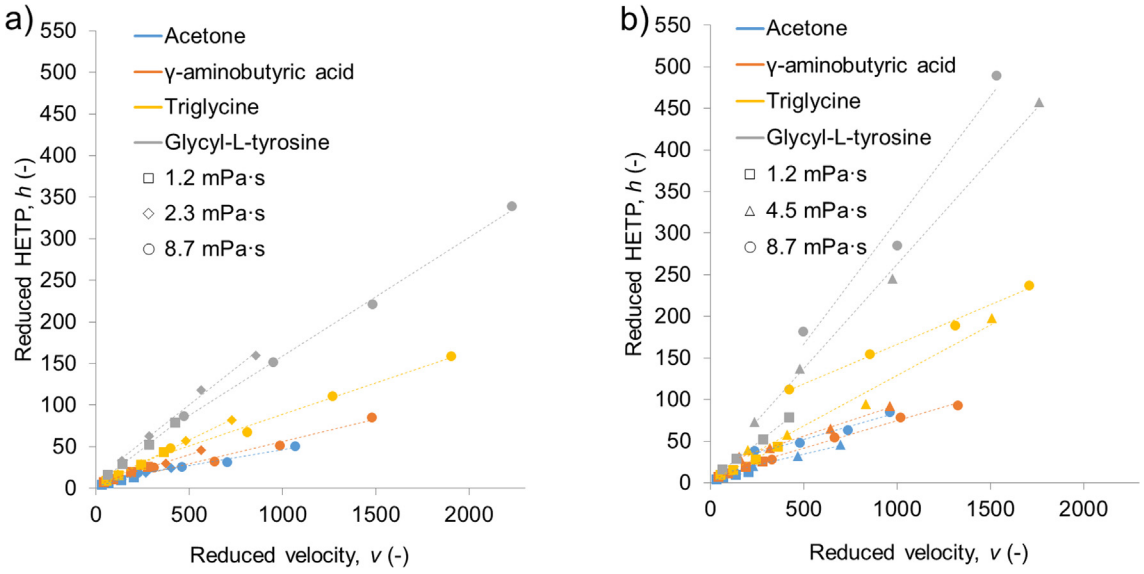

Fig. 4. Reduced HETP h over reduced velocity ν for pulse injections of *acetone*, *γ-aminobutyric acid*, *triglycine*, and *glycyl-L-tyrosine* in phosphate buffer at 1.2 mPa·s and (a) phosphate buffer containing sucrose at 2.3 and 8.7 mPa·s and (b) phosphate buffer containing glycerol at 4.5 and 8.7 mPa·s.

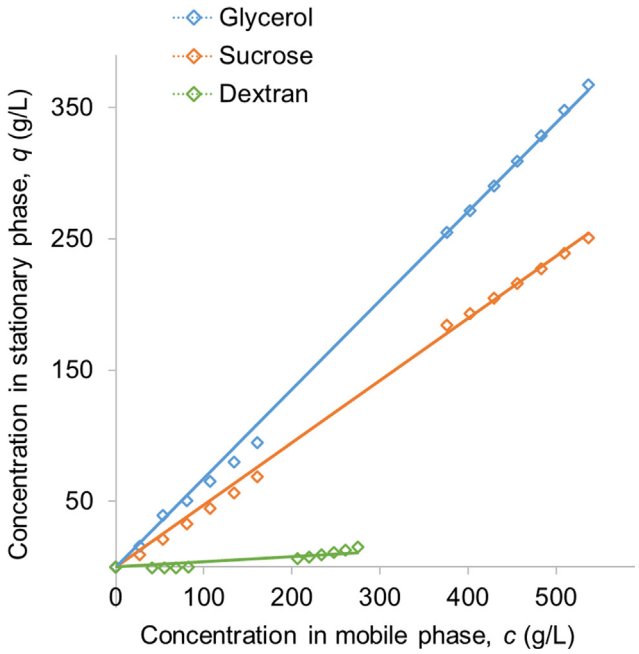

Fig. 5. Isotherms of glycerol, sucrose, and dextran.

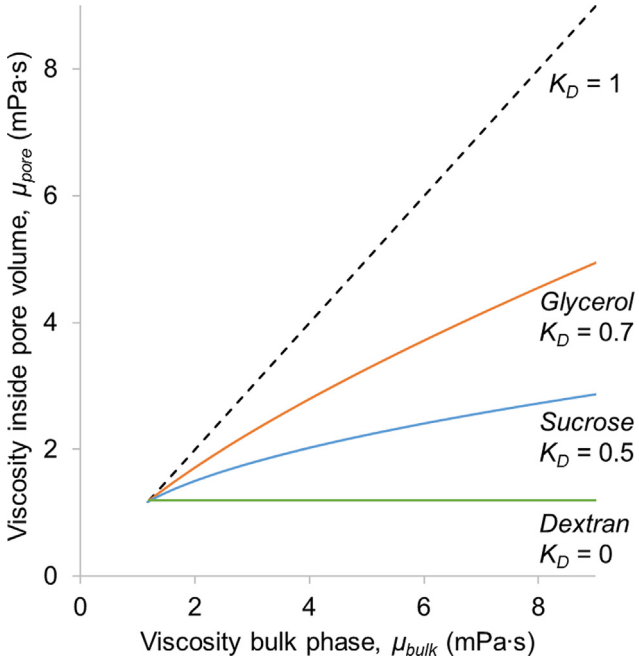

Fig. 6. Change of viscosity in pore volume μ_{pore} as function of bulk phase viscosity μ_{bulk}, based on measured partition coefficient K_D.

volume).

The dependence of mass transfer on the viscosity inside the pores is demonstrated by plotting the intraparticle diffusivity measured in mobile phase viscosified with either sucrose (closed symbols) or glycerol (open symbols) as a function of pore volume viscosity for four different target components (Fig. 7). The calculated intraparticle diffusivities are small compared to bulk diffusivities, however the range of Ω of 3 to 8% fits well with data measured for an upcoming publication and also with simulated data [23,24].

By accounting for the partition coefficient of the mobile phase viscosifying agent the respective intraparticle diffusivities line up well for each molecule, independent of the mobile phase viscosifying agent used. In all measurements *glycyl-L-tyrosine* was retained by an unknown

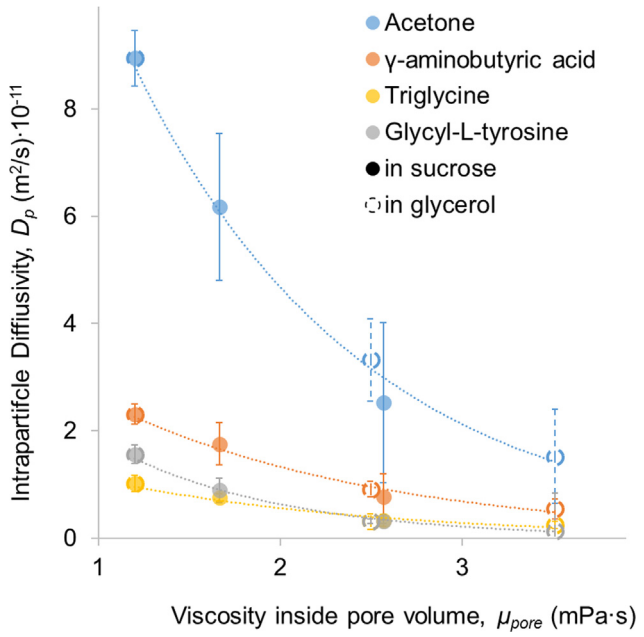

Fig. 7. Intraparticle diffusivities of *acetone, γ-aminobutyric acid, triglycine,* and *glycyl-L-tyrosine* as function of viscosity inside pore volume due to sucrose (closed symbols) and glycerol (open symbols). Error bars show 95% confidence interval.

mechanism, therefore the calculated intraparticle diffusivity is larger than for triglycine at low intraparticle viscosity, based on their respective molecular size alone, the opposite relationship was expected. The dependence of mass transfer on the viscosity inside the pores is further demonstrated by viscosifying the mobile phase with dextran, a molecule so large it does not have any access to the pore volume ($K_D = 0$). The influence of the mobile phase viscosifying agents partition coefficient K_D becomes visible when the relative intraparticle diffusivity of *triglycine* is plotted against K_D. Fig. 8 compares the intraparticle diffusivity measured at different viscosities due to glycerol, sucrose and dextran to intraparticle diffusivity measured in non-viscosified conditions. The reduction of D_p is greatest for glycerol, the smallest viscosifier molecule with the largest K_D. At the same bulk mobile phase viscosity, D_p is greater in mobile phase viscosified with sucrose because the viscosity in the pores is lower. For mobile phases viscosified with dextran to 4.5 mPa·s and 8.0 mPa·s, no significant change in D_p was measured because the viscosity in the pores stayed the same. Additionally to measured data, two calculated values for D_p were added to Fig. 8, based on the measured change of D_p with pore viscosity (open symbols). The difference intraparticle diffusivity shows the dependence of mass transfer resistance on the accessible fraction of pore volume for the viscosifying agent. The error bars show the 95% confidence intervals based on the uncertainty of the *van Deemter* slopes. For *acetone* and *γ–aminobutyric acid*, measured intraparticle diffusivity in sucrose and glycerol behaved similar to *triglycine*. Intraparticle diffusivity is not the only mass transfer to be considered, but it is the main bottleneck to efficient column design in many chromatographic applications at scale. Accurate data of change in overall mass transfer with viscosity can be used to design chromatographic systems.

4.3. System design based on bulk mobile phase viscosity

System sizes were calculated for input streams with different viscosities caused by changes in viscosifier concentration. The change in concentration reflected on the stream volume, which was calculated for viscous streams of 8.7 mPa·s diluted down to 1.2 mPa·s, on the basis of a throughput of 10 m/h at 1.2 mPa·s. For the estimation of system size with changing viscosity due to changing concentration, three

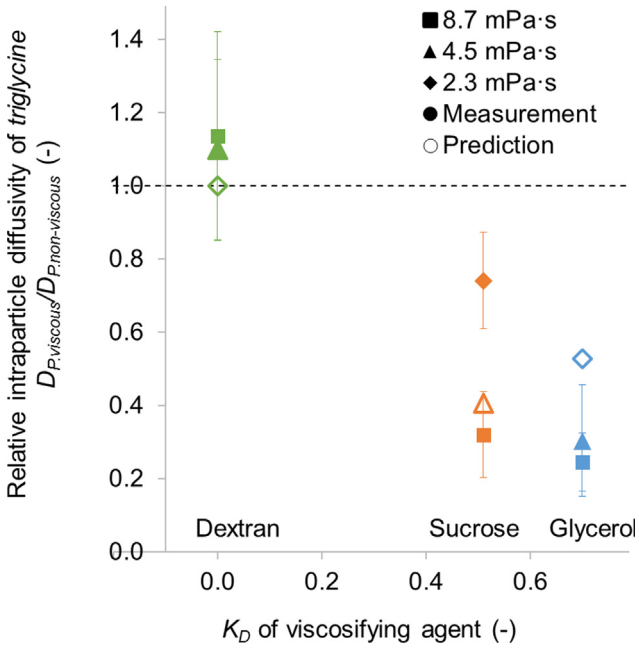

Fig. 8. Intraparticle diffusivity D_p of *triglycine* in mobile phases of 2.3 mPa·s, 4.5 mPa·s, and 8.7 mPa·s bulk viscosity with sucrose, glycerol, or dextran as viscosifying agent, relative to D_p in phosphate buffer. Closed symbols represent measured D_p, open symbols show interpolated values, based on measured intraparticle diffusivities.

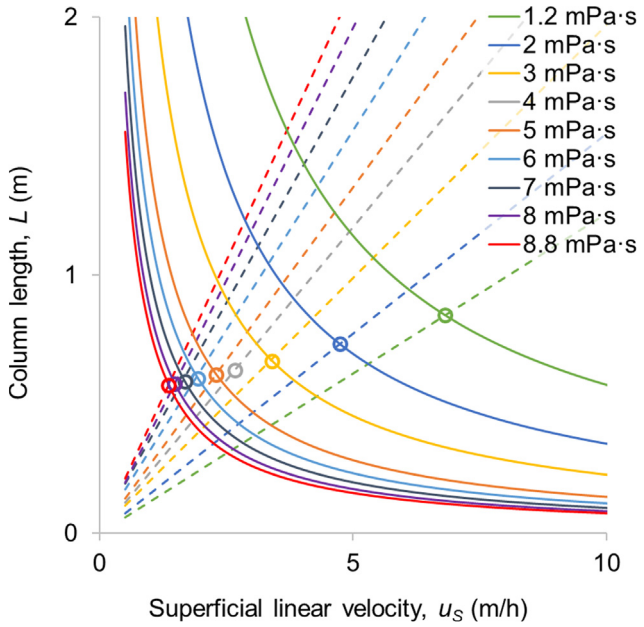

Fig. 9. Calculated column length L for a range of bulk viscosities at different linear superficial velocities u_S. Solid lines present constant pressure drop Δp (5 bar), dashed lines present a constant number of theoretical plates N (N = 100) for *triglycine* in sucrose. Intersections, marked with circles, show column length L and linear velocity u_S at which all operating conditions are met.

relationships needed to be known: viscosity of an input stream as a function of concentration, pressure drop over a column bed as function of viscosity and velocity, and *HETP* as function of viscosity and velocity. The first relationship can be found in literature for most mobile phases and is easily measured in other cases. The second relationship can be accurately calculated with Eq. (4) for non-compressible stationary phases, but the third relationship was not found in literature and was therefore measured in this work (Section 4.1).

The influence of bulk viscosity on system size is illustrated in the following via the separation of two minor components (target component *triglycine* and a component which is not retained by the resin) in a viscous medium (sucrose solution). Three important assumptions were made for the design: first, the target component did not influence mobile phase viscosity. Second, the stationary-phase was non-compressible, leading to constant bed height and porosity, independent of column diameter and pressure drop. And third, the required number of plates stayed constant, even though differences in peak shape were observed. Analogue calculations for other target components and mobile phases viscosified through glycerol or dextran were made and their results will also be discussed. For a variety of bulk viscosities and a constant pressure drop Δp, the column length L was calculated as a function of linear superficial velocity u_S with Eq. (7) (solid lines in Fig. 9). Further, for the same bulk viscosities and a constant number of plates N, the required L was calculated as a function of u_S with Eq. (8) (striped lines in Fig. 9). Calculation of column length from N required *HETP* as an input, which was measured for three different viscosities (as discussed in Section 4.1). The slope of the *van Deemter* curve changed linearly with bulk viscosity, which allowed interpolation between measured data points to calculate the slope of *van Deemter* curves at any viscosity, within the measured range. Intersections in Fig. 9, marked with circles, show L and u_S for different viscosities at required operation parameters. With increasing viscosity, L and u_S were reduced, maintaining a constant pressure drop and number of plates. From the determined intersections in Fig. 9, column dimensions were calculated as described in Section 2.2, taking into account an increase in stream volume, as concentration decreased through dilution.

Fig. 10a shows column volume as a function of bulk viscosity for mobile phases viscosified with sucrose, glycerol, and dextran and *triglycine* as target components, Fig. 10b column area A and column length L, for the same data. Change in column volume was dictated by the effect viscosity had on overall mass transfer. The change of pressure drop per column length was largely balanced through changes in the ratio of column area to column length.

With decreasing viscosity, from 8.7 mPa·s until around 2.5 mPa·s, column volume stayed more or less constant. The minute changes in column volume at higher viscosities were well within the margin of error attributable to the uncertainty encountered when measuring *van Deemter* curves at higher viscosities. Dilution to viscosities lower than 2.5 mPa·s, led to drastic increase in column volume (Fig. 10a). In the region of low viscosities, relatively large changes in stream dilution and thus stream volume and viscosifier concentration, had little impact on feed viscosity and mass transfer resistance. In a scenario where streams are diluted before chromatographic separation, the results show dilution down to a viscosity of around 2.5 mPa·s would have little to no effect on overall column volume. Dilution beyond 2.5 mPa·s would result in drastically larger column volumes.

For all target components, change in column volume with viscosity was similar, resulting in a more or less constant column volume at viscosities larger than approximately 2.5 mPa·s. Also for different viscosifiers, change in column volume followed the same overall trend, with differences in the range of 2 through 3 mPa·s. These differences are due to the difference in viscosity at the same viscosifier concentration and therefore stream volume reduction. With dextran as mobile phase viscosifier for example, measured *van Deemter* slopes are less sensitive to viscosity changes but viscosity is more sensitive to concentration changes. The sum of these two effects lead to a larger column volume with dextran as viscosifying agent in the range of 2 through 3 mPa·s, in comparison to sucrose or glycerol.

For viscosities larger than about 2.5 mPa·s, where overall column volume did not change with stream viscosity, changing viscosifier concentration still affected column length L and column area A (Fig. 10b).

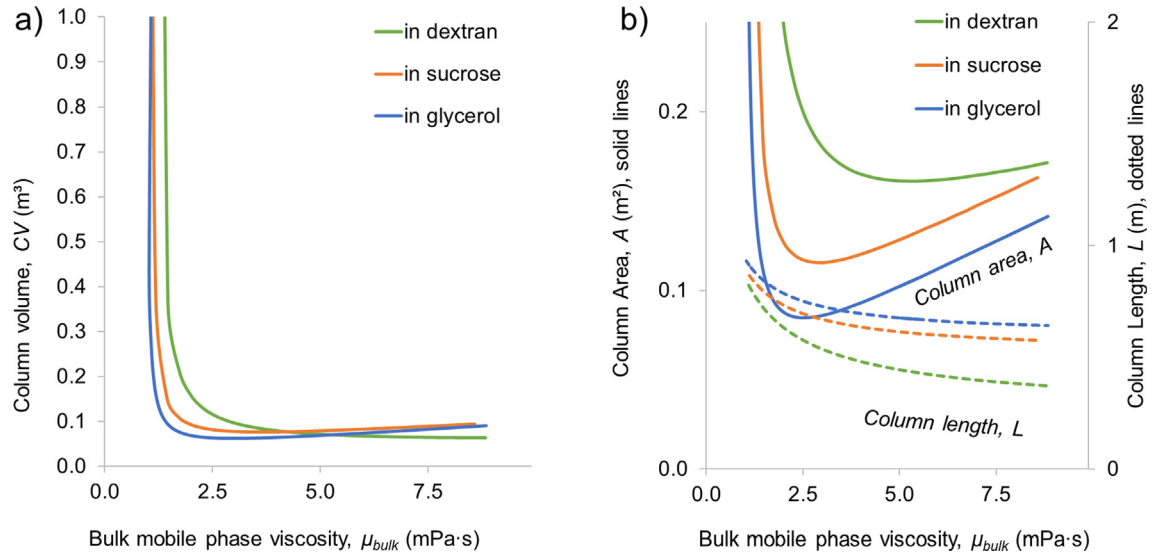

Fig. 10. (a) Column volume *CV* and (b) Column area *A* (solid line) and column length *L* (dotted line) as a function of bulk mobile phase viscosity μ_{bulk}, for constant number of plates and pressure drop for *triglycine* viscosified with dextran, sucrose, or glycerol.

With initial dilution of the stream, linear velocity increased such, that column area decreased in order to accommodate both increasing stream volume and mass transfer, while the length of the column increased. Diluting further than about 2.5 mPa·s, led to an increase in column area, required to accommodate the large stream volumes at low velocities. With larger viscosifying agents, columns became shorter and wider.

5. Conclusions

This work shows *HETP* measurements in packed bed chromatography for a range mobile phase viscosities. The results were used to explain the dependence of *HETP* on the viscosity predominant in pore space, rather than in the bulk mobile phase and further to determine the change in column size and geometry for given process parameters when streams are concentrated. With increasing viscosity each *van Deemter* curve showed an increase in slope. Mass transfer in mobile phases with sucrose, glycerol, or dextran differed, even with identical bulk viscosities, due to difference in viscosity in the pore volume. Larger molecules penetrate the pore volume to a smaller extend and have less influence on the diffusion inside the pores, which in preparative chromatography usually is the main resistance to mass transfer. Correction for viscosifier penetration into pore volume via the partition coefficient K_D, enabled the comparison and calculation of behavior for different viscosifying agents. The data showed that viscosity inside pore volume should be taken into account rather than only the viscosity of the bulk mobile phase. In case the target molecule is intrinsically viscous the difference between the viscosity inside and outside will be based on the same phenomena. The insights provided in this study can help taking viscosity differences into account when selecting a resin for a separation process. If the resin is selected such that it largely excludes the viscosity causing molecules from the pore space, mass transfer resistance inside the pores is reduced greatly and processes can be designed more efficiently.

Calculations for the influence of feed viscosity on system dimensions showed that column volume is more or less independent of stream viscosity in a viscosity range from 8.7 mPa·s down to about 2.5 mPa·s. With dilution, columns get longer and thinner, but the overall volume stays near constant. Upon further dilution, column volume is increased drastically, as viscosity becomes less sensitive to concentration changes. The difference of column volume for different viscosifying agents is not pronounced as system size is mostly dependent on the slope of *van Deemter* curves as function of viscosity. Column dimensions however do differ between viscosifying agents, tending towards larger column areas and shorter columns with viscosifying molecule size. For the estimation of process economics, column geometry can be used as an indicator for unit costs, as the logarithm of unit costs generally behaves linearly to the logarithm of a unit operations required area [2].

CRediT authorship contribution statement

A. Schultze-Jena: Conceptualization, Methodology, Investigation, Formal analysis, Writing - original draft, Data curation. **M.A. Boon:** Conceptualization, Supervision, Writing - review & editing. **R.C. Vroon:** . **P.J.Th. Bussmann:** Conceptualization, Supervision, Writing - review & editing. **A.E.M. Janssen:** Supervision, Writing - review & editing. **A. van der Padt:** Supervision, Writing - review & editing.

Declaration of Competing Interest

The authors declare that they have no known competing financial interests or personal relationships that could have appeared to influence the work reported in this paper.

Acknowledgements

The authors would like to thank Fleur Crielaard and Nina Kosten for their work on this project and Victor Aguirre Montesdeoca for his advice. This research took place within the framework of the Institute for Sustainable Process Technology ISPT (Amersfoot, NL). The authors would like to thank the *ISPT* for their support, together with Unilever (Vlaardingen, NL), FrieslandCampina Research (Amersfoort, NL), DSM (Delft, NL) and Cosun Food Technology (Roosendaal, NL) for their financial support and interest in this project.

Appendix A. Supplementary material

Supplementary data to this article can be found online at https://doi.org/10.1016/j.seppur.2019.116386.

References

[1] H. Schmidt-Traub, M. Kaspereit, S. Engell, A. Susanto, A. Epping, A. Jupke, Model-based design, optimization, and control, preparative chromatography, Wiley-VCH Verlag GmbH Co KGaA (2012) 425–518.

[2] G. Guiochon, D.G. Shirazi, A. Felinger, A.M. Katti, Fundamentals of Preparative and Nonlinear Chromatography, Academic Press, 2006.
[3] G. Guiochon, The limits of the separation power of unidimensional column liquid chromatography, J. Chromatogr. A 1126 (2006) 6–49.
[4] E.J. Fernandez, T.T. Norton, W.C. Jung, J.G. Tsavalas, A column design for reducing viscous fingering in size exclusion chromatography, Biotechnol. Prog. 12 (1996) 480–487.
[5] A. Seidel-Morgenstern, M. Schulte, A. Epping, H. Schmidt-Traub, M. Schulte, A. Seidel-Morgenstern, Fundamentals and general terminology, preparative chromatography, Wiley-VCH Verlag GmbH Co KGaA (2012) 7–46.
[6] G. Carta, A. Jungbauer, Adsorption kinetics, protein chromatography, Wiley-VCH Verlag GmbH Co KGaA (2010) 161–199.
[7] B. Coquebert de Neuville, A. Tarafder, M. Morbidelli, Distributed pore model for bio-molecule chromatography, J. Chromatogr. A 1298 (2013) 26–34.
[8] F. Gritti, G. Guiochon, Mass transfer kinetics, band broadening and column efficiency, J. Chromatogr. A 1221 (2012) 2–40.
[9] Y. Yao, A.M. Lenhoff, Determination of pore size distributions of porous chromatographic adsorbents by inverse size-exclusion chromatography, J. Chromatogr. A 1037 (2004) 273–282.
[10] P. DePhillips, A.M. Lenhoff, Pore size distributions of cation-exchange adsorbents determined by inverse size-exclusion chromatography, J. Chromatogr. A 883 (2000) 39–54.
[11] R.C. Reid, J.M. Prausnitz, B.E. Poling, The properties of gases and liquids; 1987.
[12] S. Ergun, Fluid flow through packed columns, Chem. Eng. Prog. 48 (1952).
[13] J.J. Stickel, A. Fotopoulos, Pressure-flow relationships for packed beds of compressible chromatography media at laboratory and production scale, Biotechnol. Prog. 17 (2001) 744–751.
[14] A. Schultze-Jena, M.A. Boon, P.J.T. Bussmann, A.E.M. Janssen, A. van der Padt, The counterintuitive role of extra-column volume in the determination of column efficiency and scaling of chromatographic processes, J. Chromatogr. A 1493 (2017) 49–56.
[15] J.J. Baeza-Baeza, S. Pous-Torres, J.R. Torres-Lapasió, M.C. García-Álvarez-Coque, Approaches to characterise chromatographic column performance based on global parameters accounting for peak broadening and skewness, J. Chromatogr. A 1217 (2010) 2147–2157.
[16] A.J. Alexander, T.J. Waeghe, K.W. Himes, F.P. Tomasella, T.F. Hooker, Modifying conventional high-performance liquid chromatography systems to achieve fast separations with Fused-Core columns: a case study, J. Chromatogr. A 1218 (2011) 5456–5469.
[17] F. Gritti, A. Felinger, G. Guiochon, Influence of the errors made in the measurement of the extra-column volume on the accuracies of estimates of the column efficiency and the mass transfer kinetics parameters, J. Chromatogr. A 1136 (2006) 57–72.
[18] J.A. Vente, H. Bosch, A.B. de Haan, P.J.T. Bussmann, Evaluation of sugar sorption isotherm measurement by frontal analysis under industrial processing conditions, J. Chromatogr. A 1066 (2005) 71–79.
[19] M.V. Galmarini, R. Baeza, V. Sanchez, M.C. Zamora, J. Chirife, Comparison of the viscosity of trehalose and sucrose solutions at various temperatures: effect of guar gum addition, LWT - Food Sci. Technol. 44 (2011) 186–190.
[20] N.-S. Cheng, Formula for the viscosity of a glycerol-water mixture, Ind. Eng. Chem. Res. 47 (2008) 3285–3288.
[21] S. Xie, S. Zhang, X. Qiu, C. Yi, Y. Hu, F. Li, J. Quan, Sugaring-out effects of sucrose and glucose on the liquid-liquid equilibria for the (water + acetone + 1-butanol + ethanol) system, J. Chem. Eng. Data 60 (2015) 2434–2441.
[22] H. Katayama, T. Satoh, Liquid-liquid equilibria of three ternary systems: glycerol + acetone + water, glycerol + 1, 4-dioxane + water, and glycerol + acetonitrile + water, Solvent Extr. Res. Dev., Jpn. 22 (2015) 1–15.
[23] J.J. Meyers, O.K. Crosser, A.I. Liapis, Pore network modelling of affinity chromatography: determination of the dynamic profiles of the pore diffusivity of β-galactosidase and its effect on column performance as the loading of β-galactosidase onto anti-β-galactosidase varies with time, J. Biochem. Bioph. Methods 49 (2001) 123–139.
[24] J.J. Meyers, A.I. Liapis, Network modeling of the intraparticle convection and diffusion of molecules in porous particles packed in a chromatographic column, J. Chromatogr. A 827 (1998) 197–213.